Received: 29 October 2018 | Revised: 10 February 2019 | Accepted: 13 February 2019

DOI: 10.1002/hbm.24555

WILEY

RESEARCH ARTICLE

Resting-state fMRI effective connectivity between the bed nucleus of the stria terminalis and amygdala nuclei

David Hofmann | Thomas Straube

Institute of Medical Psychology and Systems Neuroscience, University Hospital Muenster, Muenster, Germany

Correspondence
David Hofmann, Institute of Medical Psychology and Systems Neuroscience, University Hospital Muenster, Von-Esmarch-Straße 52, D-48149 Muenster, Germany.
Email: davidhofmann@uni-muenster.de

Funding information
German Research Foundation, Grant/Award Number: DFG: SFB/TRR 58: C06, C07

Abstract

The bed nucleus of the stria terminalis (BNST) and the laterobasal nucleus (LB), centromedial nucleus (CM), and superficial nucleus (SF) of the amygdala form an interconnected dynamical system, whose combined activity mediates a variety of behavioral and autonomic responses in reaction to homeostatic challenges. Although previous research provided deeper insight into the structural and functional connections between these nuclei, studies investigating their resting-state functional magnetic resonance imaging (fMRI) connectivity were solely based on undirected connectivity measures. Here, we used high-quality data of 391 subjects from the Human Connectome Project to estimate the effective connectivity (EC) between the BNST, the LB, CM, and SF through spectral dynamic causal modeling, the relation of the EC estimates with age and sex as well as their stability over time. Our results reveal a time-stable asymmetric EC structure with positive EC between all amygdala nuclei, which strongly inhibited the BNST while the BNST exerted positive influence onto all amygdala nuclei. Simulation of the impulse response of the estimated system showed that this EC structure shapes partially antagonistic (out of phase) activity flow between the BNST and amygdala nuclei. Moreover, the BNST-LB and BNST-CM EC parameters were less negative in males. In conclusion, our data points toward partially separated information processing between BNST and amygdala nuclei in the resting-state.

KEYWORDS

amygdala, bed nucleus of the stria terminalis, dynamic causal modeling, effective connectivity, Human Connectome Project, impulse response, resting-state fMRI

1 | INTRODUCTION

The human brain is a complex system consisting of dynamically interconnected networks. In this vast interacting set of networks, the amygdala and the bed nucleus of the stria terminalis (BNST) play crucial roles with regard to the assessment of the value of internal and external stimuli and the adaptive initiation of behavioral and autonomic responses in reaction to homeostatic challenges (for reviews, see Davis, Walker, Miles, & Grillon, 2010; Pessoa, 2011). The amygdala can be roughly divided into three sets of nuclei, the laterobasal nucleus (LB), centromedial nucleus (CM), and superficial nucleus (SF). Research about the functional specialization of these nuclei is ongoing, but several lines of evidence suggest that the LB is vital for an organism to associate specific sensory attributes of a stimulus to memories as well as learn and access its momentary value (Cardinal, Parkinson, Hall, & Everitt, 2002; Pessoa, 2011). The CM, on the other hand, has been proposed to mediate general behavioral, attentional as well as affective and autonomic consequences of an aversive or rewarding stimulus in a flexible manner (Balleine & Killcross, 2006; Fadok, Markovic, Tovote, & Lüthi, 2018). The SF is a part of the medial amygdala, receiving information from the olfactory system, driving innate odor-driven behaviors in animals (Maras & Petrulis, 2008; Root, Denny, Hen, & Axel, 2014) and, in humans, seems to contribute to complex socioaffective information processing (Goossens et al., 2009; Koelsch et al., 2013; Skouras, Gray, Critchley, & Koelsch, 2014). The BNST is located in the basal forebrain and can be roughly divided into an anterior and posterior nucleus. It has been found to be involved in a large variety of functions including mood regulation, arousal, motivation for social behavior and social attachment (Lebow & Chen, 2016). More generally, Lebow and Chen (2016) proposed that the BNST is essential for valence surveillance through processing of salient information that is based on monitoring the physical and social contexts.

Both BNST and amygdala are strongly interconnected on a structural level (Sah, Faber, Lopez De Armentia, & Power, 2003; Waraczynski, 2016). The BNST is connected to the amygdala via the ventral amygdalofugal pathway and the stria terminalis (Sun, Roberts, & Cassell, 1991) and thus shows structural connections to the LB, CM, and SF (Cooke & Simerly, 2005; Oler et al., 2017; Weller & Smith, 1982). Particularly, the CM and the BNST have been proposed to belong to the medial extended amygdala due to their high similarity with respect to embryological origin, cell type, afferent, and efferent connections (Bienkowski & Rinaman, 2013; Bupesh, Abellán, & Medina, 2011; Dong, Petrovich, & Swanson, 2001; Sah et al., 2003) and timing of impulses to the brainstem (Nagy & Paré, 2008). Because of their interconnectedness and similarity, research indicates that the BNST and the amygdala nuclei work in accordance to mediate a variety of behaviors, in particular anxiety- and fear-related behaviors (Davis et al., 2010). For example, projections from the CM to the BNST can increase measures of anxiety in mice (Ahrens et al., 2018) and precise optogenetic stimulation of LB terminals in the CM induces anxiolytic effects, whereas inhibition results in an increase in anxiety-related behaviors in mice (Tye et al., 2011).

Moreover, photostimulation of LB projections to the CM has been found to mediate negative reinforcement (Namburi et al., 2015). Additionally, stimulation of LB inputs to the anterodorsal nucleus of the BNST increases behavioral (avoidance) and physiological (respiratory rate) measures of anxiety in mice, whereas inhibition has the opposite effect of decreasing anxiety measures (Kim et al., 2013). Also, the interactions of amygdala nuclei with each other is crucial for a well functioning organism. For example, it has been found that the CM influences learning in the LB (Yu et al., 2017). Finally, the SF has been found to be connected to the BNST (Cooke & Simerly, 2005) relaying chemosensory and hormonal information (Been & Petrulis, 2011). This data suggest that the amygdala nuclei and BNST, by means of their mutual interaction, enable the organism to respond adaptively to homeostatic challenges.

However, although the structural connectivity between amygdala and BNST has been mapped in detail in animals (Dong et al., 2001) and in part in humans (Avery et al., 2014; Krüger, Shiozawa, Kreifelts, Scheffler, & Ethofer, 2015), there is a lack of research that investigated the mutual directional influences of these structures in humans by means of effective connectivity (EC) analysis. Resting-state functional magnetic resonance imaging (fMRI) (rsfMRI) connectivity analysis offers deeper insight into the connectivity structure between regions in the "task-free" brain, but to our knowledge, only a few studies investigated the rsfMRI connectivity between BNST and amygdala nuclei so far. For example, Oler et al. (2012, 2017) used resting-state functional connectivity (rsFC) analysis in humans and primates to examine the correlation between the CM and the BNST and found a positive functional connection. A recent study by Fox et al. (2018) also investigated the intrinsic fMRI-based FC between BNST and CM and its heritability in a large sample of primates. They reproduced the previous findings of Oler et al. and additionally found that the strong positive FC between CM and BNST is heritable. Similar results were reported by Avery et al. (2014) in humans who analyzed the rsFC of the BNST with the LB, CM, and SF and found significant connectivity to all subregions in agreement with their estimates of structural connections based on diffusion tensor imaging. Another study by Torrisi et al. (2015) investigated the whole-brain rsFC of BNST in 7 Tesla and likewise found positive FC to the CM as well as the LB and SF. In a follow-up study, Torrisi et al. (2018) further investigated the task-dependent changes in FC between BNST and CM in a safety versus threat condition (shock anticipation). The safety condition was used as a measure for resting-state activity, since subjects passively watched a fixation cross (as it is often done during a resting-state acquisition). Their results again showed significant positive rsFC between BNST and CM in accordance with their previous findings. Another study by Tillman et al. (2018) similarly investigated the whole-brain rsFC of the BNST and the CM and found positive FC of the BNST with the central and medial nuclei of the amygdala. These results point toward a positive interconnectedness between BNST and all amygdala nuclei. However, all the studies used FC analysis, which is based on symmetric correlations and thus can not establish the direction of connectivity (Friston, 2011). In other words, measures of FC are not able to infer true coupling, because it is a mapping from consequences to causes based on statistical dependencies (Friston, 2011). For example, two regions can show substantial FC despite the absence of any true connection, just because of a common input from a third region (Friston, 2011). Moreover, since correlations depend on the level of observation noise, changes in FC arise by merely varying the signal-to-noise ratio, for example, by increasing the number of time points or the sample size (Friston, 2011). Moreover, changes in FC also arise by changing the amplitudes of neuronal fluctuations (Friston, 2011).

To overcome these limitations, we used dynamic causal modeling to estimate the EC between BNST and amygdala nuclei. In contrast to FC, EC estimation through dynamic causal modeling rests on generative (state-space) models with a biologically realistic hemodynamic observer function, that map causes to consequences (Friston, 2011; Friston, Harrison, & Penny, 2003). Therefore, EC estimation based on a dynamic causal model (DCM) is able to offer insight into the model-based connectivity structure between regions, rather than their statistical dependencies that can be influenced by several factors that do not result from real changes in the underlying coupling. In order to assure a robust estimation of the DCM, we used data from the Human Connectome Project (HCP) of 391 unrelated healthy subjects with 2,400 time points. Additionally, to investigate the stability of the EC parameters over time, we repeated our analysis with data from a second session that was acquired on a different day. We additionally calculated partial correlations between BNST and amygdala nuclei.

We hypothesized that: (a) the results from the partial correlations will reproduce the findings from previous studies that showed positive correlations between all structures and (b) the EC estimates at least partially reflect previous results, but show a directed and hence richer connectivity structure. However, since to our knowledge, this is the first study investigating the EC between these structures, we could only formulate a weak hypothesis about the EC between BNST and amygdala nuclei based on results from undirected FC. Moreover, we expected the connectivity parameters to be stable over both sessions.

Furthermore, the influence of age and sex on the connectivity parameters has not been explicitly investigated in previous studies. Given that the BNST has been found to be sexually dimorphic (Allen & Gorski, 1990; Hines, Allen, & Gorski, 1992), and that the FC of the amygdala has also been found to be dependent on age and sex

(Alarcón, Cservenka, Rudolph, Fair, & Nagel, 2015; Engman, Linnman, Van Dijk, & Milad, 2016; Gabard-Durnam et al., 2014), we expected that these factors also have differential effects on the EC estimates.

In addition to the estimation of the EC parameters, we wanted to explore the time-dependent dynamics of BNST and amygdala, which is generated by the mutual influences between all the nuclei. That is, after the estimation of the EC parameters, we simulated the impulse response of the estimated DCM equations, without a hemodynamic observer function and noise term, to an impulse input into the LB. The impulse response of a linear time-invariant system provides deeper insight into the information propagation within a system in reaction to a brief external input (Hespanha, 2018).

This article is structured as follows: We will first describe the methods used in this study in detail, followed by a presentation of the results of the EC parameter estimations and their relation to age and sex. This is followed by the results of the simulated impulse response. We finally discuss the role of the estimated EC parameter structure in shaping information processing between the BNST and amygdala nuclei. In Appendix S1 (Supporting Information), the reader will find more information about the partial correlation analysis, impulse response estimation, additional DCMs separated by hemisphere, as well as more detailed outputs of the DCM estimation.

2 | METHODS

2.1 | Sample

From the final 1,206 HCP subjects, we selected all subject that were unrelated (n = 457 in total) and excluded all subjects that had incomplete resting-state data (n = 66 exclusions) or missing age and sex information (n = 0). Our sample thus consisted of 391 unrelated healthy subjects (mean age: 28 ± 3.6 years, 172 males and 219 females). We did not exclude any additional subjects since the HCP sample already consisted of subjects that were free of neurodevelopmental, neuropsychiatric and neurologic disorders and met a series of further inclusion criteria (see Van Essen et al., 2013). The data are publicly available at the HCP online database (https://www.humanconnectome.org). Information on the age of the participants was obtained after acceptance of the open and restricted access agreements put forward by the Consortium of the Washington University-Minn HCP (WU-Minn HCP). Subject recruitment procedures and informed consent forms were approved by the WU institutional review board. All data presented in this article are not identifiable.

2.2 | Data acquisition

The data were acquired on a 3 Tesla Skyra Siemens system using a 32-channel head coil, a customized SC72 gradient insert (100 mT/m) and a customized body transmit coil. The anatomical images were acquired with a high resolution (0.7 mm isotropic) T1-weighted three-dimensional magnetization prepared rapid gradient echo sequence (repetition time 2400 ms, echo time 2.14 ms, flip angle: 8°, field of view 224 × 224 mm^2) and the functional images were acquired using a multiband gradient echo EPI sequence (repetition time 720 ms, echo time 33.1 ms, resolution 2 mm isotropic, 72 oblique axial slices, flip angle 52°, field of view 208 × 108 mm^2, matrix 104 × 90, echo spacing 0.58 ms, 1,200 images per rsfMRI run) (Glasser et al., 2016). Specifically, rsfMRI data were acquired in four runs of approximately 15 min each, two runs in one session, and two in another session with eyes open with a relaxed fixation on a projected bright crosshair on a dark background. Within each session, oblique axial acquisition alternated between phase encoding in a right-to-left direction in one run and phase encoding in a left-to-right direction in the other run.

2.3 | Data preprocessing

Our data consisted of the extended ICA-FIX denoised resting-state fMRI data sets from two different sessions acquired on two separate days. All preprocessing of HCP data was carried out in FMRIB Software Library (FSL) and specifically designed for the HCP acquisition protocols. For a detailed description of the HCP preprocessing methods, please see Glasser et al. (2013) and Smith et al. (2013). Briefly, the minimal preprocessing pipeline for the fMRI data consisted of gradient distortion correction to remove spatial distortions, followed by realignment of volumes to compensate for subject motion, coregistration of the fMRI data to the structural image, nonlinear registration to MNI space, intensity normalization to a mean of 10,000, bias field removal and masking of the data with a final brain mask. No overt volume smoothing was applied, and special care was taken to minimize smoothing from interpolation. After application of the minimal preprocessing pipeline, further processing was done for the resting-state data. For this, the data were cleaned of structured noise by combining independent component analysis (ICA) with the automated component classifier tool FIX (FMRIB's ICA-based X-noisifier) (Griffanti et al., 2014; Salimi-Khorshidi et al., 2014). FIX classifies the ICA-detected components into "good" and "bad" (artifactual) and has been specifically trained on HCP data. The artifactual components were then removed in a non-aggressive manner, that is, removing only the unique variance associated with each component. This approach avoids removing potential variance of interest (Smith et al., 2013). Finally, head motion time series were regressed out by using a 24 confound time series containing the six rigid-body parameter time series, their temporal derivatives as well as the resulting 12 regressors squared). In order to profit from the high quality of the HCP data, we did not apply any additional preprocessing steps except for filtering low-frequency scanner drifts with a high-pass filter cutoff of 200 s. For the subsequent DCM analysis, no additional filtering in the frequency range between 0.01 and 0.1 Hz was applied since the spectral DCM-based analysis explicitly models the cross-spectral density within this frequency range.

2.4 | Data preparation

Within each session, we concatenated the data of the different phase encoding directions, to obtain a data set consisting of 2,400 images for each session. Before concatenation, we first mean-centered and then variance normalized the data by dividing by the temporal *SD* of the unstructured noise. The unstructured noise temporal *SD* was obtained by first regressing out all signal components of the time series at each voxel leaving only the noise components, and then

calculating the temporal *SD* of the time series at each voxel. By this, it was ensured that the unstructured noise magnitude was distributed equally across the brain for each subject. The signal components were obtained by ICA and already included in the ICA-FIX extended data set.

2.5 | Regions of interest selection

For the subsequent DCM analysis, masks of amygdala nuclei were obtained from the Anatomy Toolbox (AT) version 2.2c (Eickhoff et al., 2005) available for statistical parametric mapping 12 (SPM12). The masks consisted of the maximum probability maps of the LB, CM, and SF (Amunts et al., 2005). The mask for the BNST was obtained from the probabilistic atlas developed by Torrisi et al. (2015). For the BNST mask, we included all voxels with at least 80% probability of being located within the BNST. All masks consisted of the regions of both hemispheres since we did not differentiate between hemispheres in the main analysis. For an overview of the selected ROIs, see Figure 1.

2.6 | Regions of interest extraction

Region of interest (ROI) time series extraction for the later DCM analysis was performed using the volume-of-interest tool included in SPM12 (v7219). ROI time series were obtained by selection of the first principal component, that is, the component that explained the most variance after calculation of a principal component analysis that included the time series of all voxels within an ROI. Before extraction, we ensured that all subjects had sufficient EPI coverage of the ROIs, which was the case for all subjects in our sample.

2.7 | Dynamic causal modeling

All analysis was done using SPM12 (v7219) in MATLAB 2017b. After extraction of the ROI time series, we calculated a one-state spectral DCM, specifying a model of EC in which all ROIs were connected with each other. Spectral DCM is a variant of DCM that is suited for the estimation of EC in resting-state fMRI data and uses a neuronally plausible model of coupled neuronal states to generate complex cross spectra (Friston, Kahan, Biswal, & Razi, 2014). In other words, the generative model is identical to the deterministic DCM used in fMRI time series analysis (Friston et al., 2003) but is used to predict the sample (second-order) cross spectra as opposed to the time series themselves. In comparison to previous approaches based on stochastic differential equations (stochastic DCM), this variant enables faster, more accurate and less computationally intensive estimation of EC (Razi et al., 2017; Razi, Kahan, Rees, & Friston, 2014). The DCM used here consists of a system of random differential equations that model neuronal interactions of the form:

$$\mathbf{x}(t) = \mathbf{A}\,\mathbf{x}(t) + \boldsymbol{v}(t) \quad (1)$$

where $\mathbf{x}(t) = [\mathbf{x}_1(t), \ \ldots\ , \mathbf{x}_4(t)]^{\mathrm{T}}$ is a column vector of hidden neuronal states for the four regions BNST, LB, CM, and SF whose activity depends on the other regions and endogenous fluctations modeled by $\mathbf{v}(t)$. The hidden states are abstract representations of neuronal activity that correspond to the amplitude of macroscopic variables, which summarize the dynamics of large neuronal populations. The endogenous fluctuations are generated from an AR(1) process with autoregression coefficient of one half. **A** is a four by four matrix with the unkown coupling coefficients between regions, that is, the EC parameters in units of Hertz to be estimated given the data. The resulting output values then serve as input to equations that generate the hemodynamic responses of each ROI. The equations that generate the hemodynamic response are not shown here. For details, see Friston et al. (2003). This DCM is then fitted to the cross spectra of the extracted ROI time courses of each subject.

2.8 | Parametric empirical Bayes for group DCM

After fitting each subject's DCM to their data, we ran a second level analysis in order to estimate the group mean and the effects of the covariates age and sex for each connectivity parameter of the model. This analysis was based on the recently developed parametric empirical Bayes (PEB) method that models connectivity at the group level by means of a hierarchical Bayesian model (Friston et al., 2016). The subject-specific connectivity estimates (consisting of the expected values and covariances) are taken to the group level by fitting a Bayesian General Linear Model to the data. Other than tests based on classical statistics, PEB uses the full posterior density over the connectivity parameters from each subject's DCM to inform results on the group level. It thus takes into account both the expected strength of the connection and its uncertainty (posterior covariance). In other words, subjects are weighted by the precision of their estimates, such that subjects with noisy estimates contribute less to the group result.

2.9 | Bayesian model reduction

Since we could base our hypothesis about the EC between BNST and amygdala nuclei only on previous evidence from studies using FC, we chose an exploratory approach by specifying a fully connected model and used Bayesian model reduction to identify the best model given the data. This was done by removing one or more connectivity parameters from the full PEB group-level model to produce reduced forms of the full model and deriving the model evidence (free energy). With this approach, it is possible to obtain the evidence and parameters of reduced models directly from the fully connected model and thus provides an efficient search of the model space by scoring each reduced model based on its model evidence or free energy (for details, see Friston et al., 2016). The models that maximize the model evidence are then selected. After model reduction, Bayesian model averaging was used to average the connectivity parameters of the best models (56 in the first session and 26 in the second session), weighted by their evidence. That is, the most probable model will contribute the most to the average. In the result section, we report the EC parameter estimates of this average over the best models.

2.10 | Impulse response simulation

After estimation of the group-level EC parameters, we simulated the (neuronal) response of the system to a Dirac impulse input into the LB, the main input station of the amygdala. To accomplish this, we

dropped the noise term in Equation 1 and replaced the unknown coefficients of matrix A by the estimated group-level EC parameters averaged over the two sessions and integrated the system (see impulse response equations in the Supporting Information for more details). Since the found EC parameters shape the internal dynamics of the system and determine the response of each region to an external input, simulation of the impulse response provides further insight into the propagation of information within the BNST-amygdala circuit.

2.11 | Calculation of partial correlations

For the calculation of the partial correlations, we first band-pass filtered the ROI time series in the frequency range from 0.01 to 0.1 Hz and then used the *partialcor* MATLAB function to obtain the partial correlation matrix for the BNST, the CM, LB, and SF. Subsequently, the correlations from each subject where Fisher *z*-transformed and a one-sample *t* test with an alpha error level of 5% was calculated for each partial correlation coefficient over all subjects.

2.12 | Robustness against hemispheric lateralization

In order to check for differences in the EC between hemispheres, we calculated a DCM for the ROIs of each hemisphere separately.

3 | RESULTS

3.1 | EC between BNST and amygdala nuclei

Our results reveal that the BNST and amygdala nuclei are fully and asymmetrically connected in the resting-state (Figure 2). In other words, a fully connected DCM explained the data best, that is, maximized the model evidence (for details, see Figures S5–S8, Supporting Information). All amygdala nuclei were positively connected with each other but showed strong negative EC to the BNST. The BNST, on the other hand, showed positive EC to all amygdala nuclei. In detail, the BNST showed the strongest EC to the LB followed by the SF and the CM. The CM showed the strongest positive EC to the LB and the SF and the weakest negative EC to the BNST. The LB showed the strongest EC to the SF and the CM and the strongest negative EC to the BNST. The SF showed the strongest EC to the LB followed by the CM and negative EC to the BNST. The results were stable over the two sessions, although the magnitude of the EC parameters in the second session was comparatively smaller. The CM showed the strongest self-inhibition, followed by the SF in both sessions. The BNST showed the least self-inhibition in the first session, and in the second session, the LB showed the least self-inhibition.

3.2 | Age effects on EC parameters

We did not find any consistent effects of age on the EC parameters in the two sessions.

3.3 | Sex effects on EC parameters

Our results (Figure 3) showed that in the first session, compared to females, males show stronger EC from the CM to the BNST and from the LB to the BNST. Compared to males, females showed stronger EC from the SF to the BNST and from the SF to itself. However, only the CM-BNST and LB-BNST EC were reproduced in the second session.

3.4 | Impulse response of group-level DCM

Figure 4 shows the result of the impulse response of the system to an impulse into the LB (for details, see impulse response equations in the Supporting Information). As can be seen, the system displays decaying

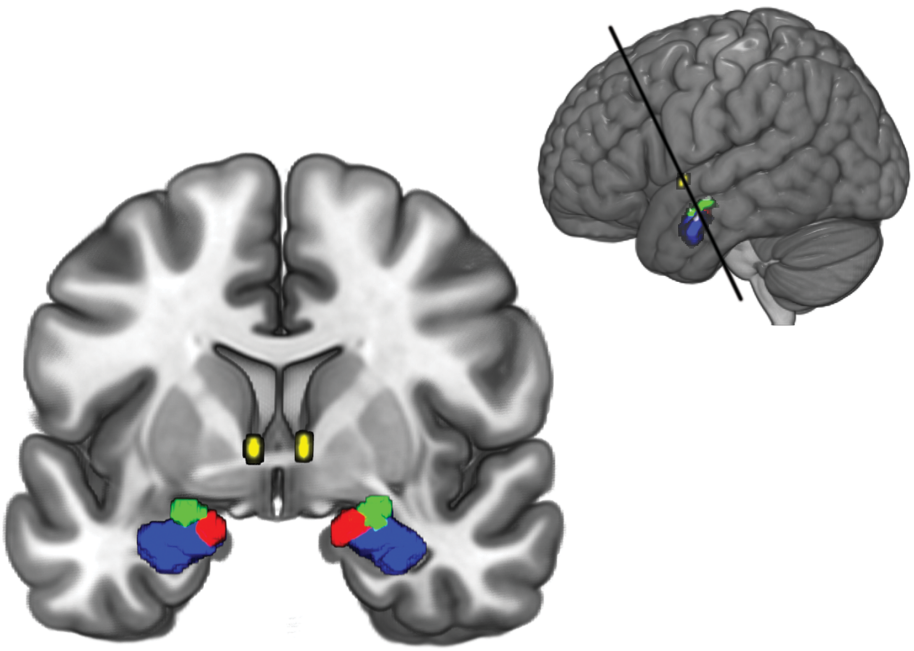

FIGURE 1 Amygdala nuclei and bed nucleus of the stria terminalis (BNST) regions of interest used in this study. The laterobasal nucleus (LB) is shown in blue, the centromedial nucleus (CM) in green, the superficial nucleus (SF) in red, and the BNST in yellow. Top right inlay shows the section [Color figure can be viewed at wileyonlinelibrary.com]

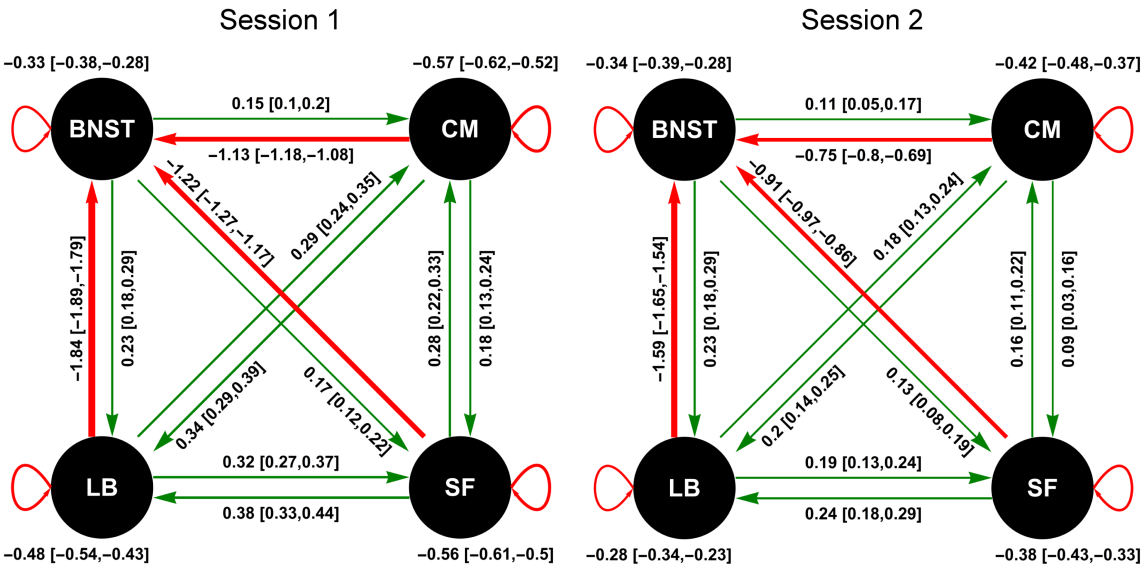

FIGURE 2 Effective connectivity (EC) between the bed nucleus of the stria terminalis (BNST), the laterobasal nucleus (LB), centromedial nucleus (CM), and superficial nucleus (SF) for the two sessions. The values show the EC estimate and its 95% credible interval in brackets. Positive EC is shown in green and negative EC is shown in red [Color figure can be viewed at wileyonlinelibrary.com]

oscillatory activity. The resulting activity flow propagates within the amygdala circuits generating in-phase activity of the LB, CM, and SF, which reaches a peak 0.8 s after stimulus onset. Concurrently, the BNST displays a large amplitude downregulation that is mediated by the strong inhibitory EC from the amygdala nuclei. The downregulation shows a peak approximately 1.7 s after stimulus onset. The decrease in BNST activity then results in negative inhibitory feedback onto all the amygdala nuclei which reaches its minimum 3.7 s after stimulus onset, the same time as the activity of the BNST is around zero. This downregulation of the LB, CM, and SF, in turn, results in strong positive feedback to the BNST, that is, increasing its activity to a maximum 5.5 s after stimulus onset. Thus, a rise in activity of the amygdala results in downregulation of the BNST, which is followed by an increase in activation later on during which the amygdala nuclei show decreased activity. As can be seen, the activity of the amygdala is maximal when the BNST activity is around zero and vice versa. The activity flow of the BNST thus shows a phase shift of approximately 90°, resulting in a partially out of phase relation to the amygdala nuclei activity. Since both structures are thus not entirely out of phase, they still display periods of overlapping activity. On the other hand, activity within the amygdala nuclei is strongly phase synchronized. Notably, the BNST shows comparatively larger activity amplitude than the amygdala nuclei and its activity takes longer to decay to zero. Note that a similar partially antagonistic activity flow also arises when an impulse is input into any other nucleus (not shown here). Thus, the partially antagonistic nature of the activity flow between BNST and

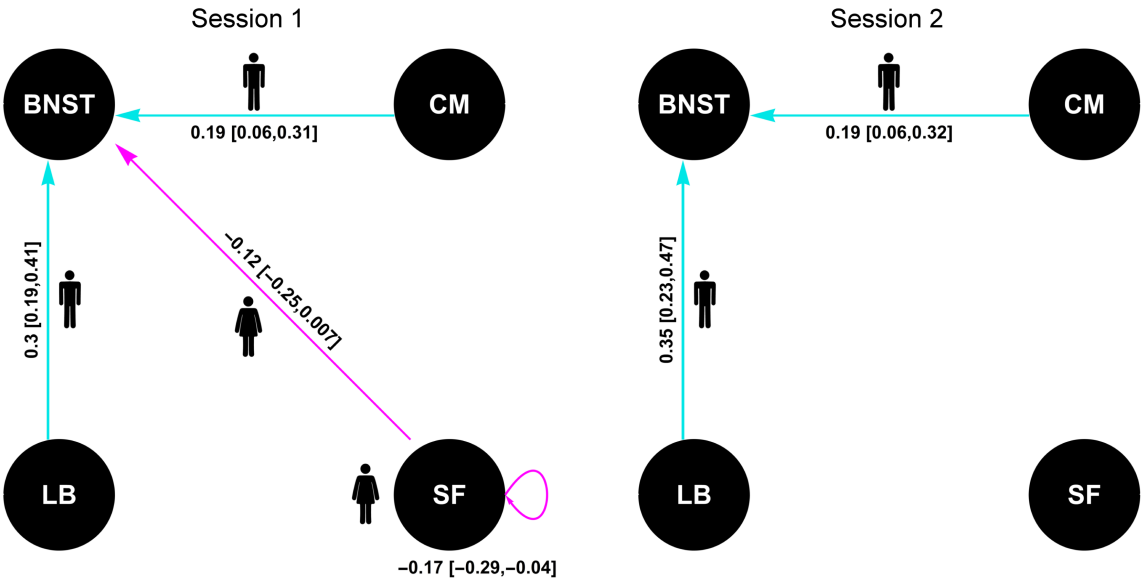

FIGURE 3 Effects of sex on effective connectivity (EC) parameters. The values show the estimate and its 95% credible interval in brackets. Larger EC in males is represented by a male symbol and shown in cyan. Larger EC in females is represented by a female symbol and shown in magenta [Color figure can be viewed at wileyonlinelibrary.com]

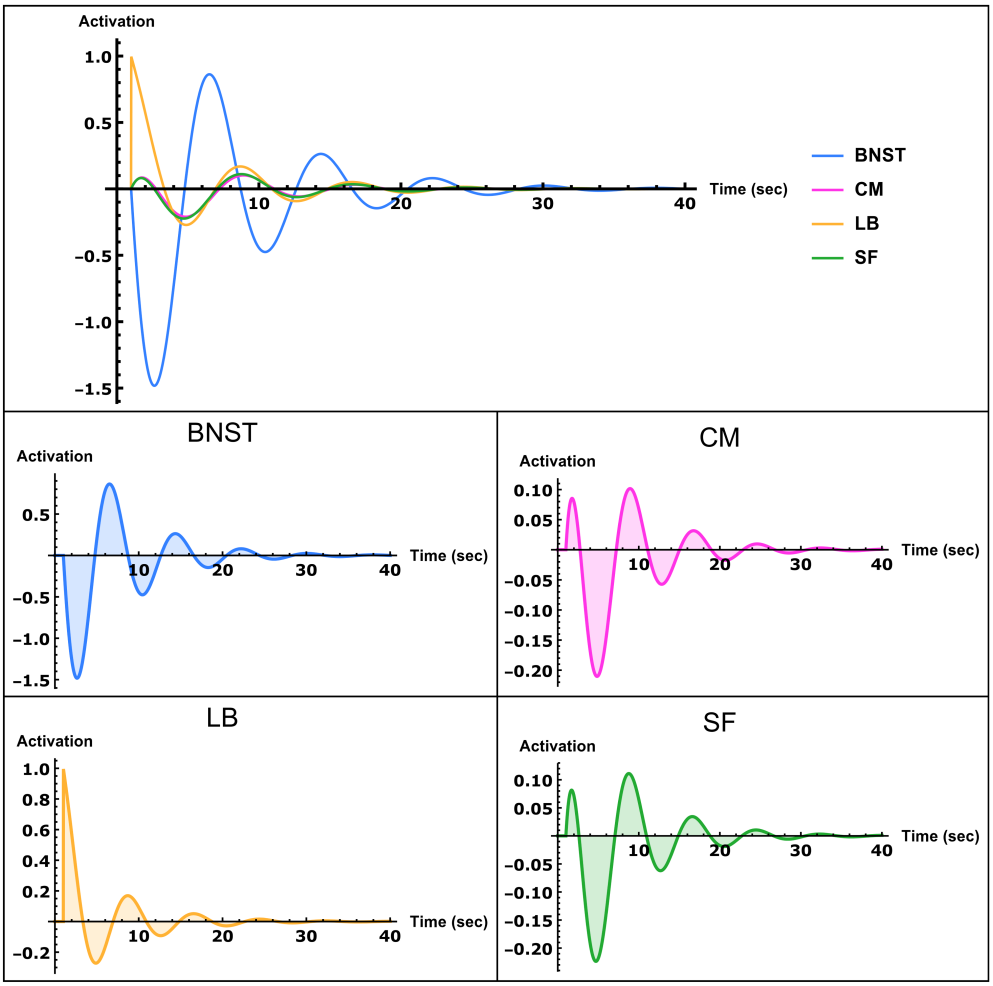

FIGURE 4 Impulse response of the group-level dynamic causal model (DCM) equations to an impulse input into the laterobasal nucleus (LB) shown over a period of 40 s. Top row: Impulse responses of all regions in one plot for an easier comparison of the magnitude of activations of each region of interest (ROI). Middle/bottom row: Impulse response of each ROI separately. Activity scale is arbitrary, but positive values indicate upregulation, whereas negative values indicate downregulation; time units are in seconds [Color figure can be viewed at wileyonlinelibrary.com]

amygdala nuclei is independent of the region which receives the impulse. This can be attributed to the strong interconnectedness between all nuclei. For example, an impulse input into the BNST would increase activation of the amygdala nuclei, which then leads to inhibitory feedback onto the BNST, resulting in inhibition of the amygdala nuclei and so forth until the activity decays. Here again, maximal activation of the amygdala leds to diminished BNST activity and vice versa. During periods where activation is not maximal, there also exists a time window of overlapping activity of both structures, resulting in partially anatgonistic activity flow.

3.5 | Partial correlations between BNST and amygdala nuclei

The results of the partial correlations are shown in Figures S1–S3 and Table S1 and S2 (Supporting Information). The partial correlations for both sessions reproduced previous research showing significant positive correlations between the BNST, the LB, CM, and SF except for a nonsignificant BNST-SF connection in the second session. The effect sizes were small with a maximum significant partial correlation of 0.16 for the CM-LB connection in the second session and a minimum of 0.007 for the BNST-CM/BNST-SF connection in the first and second sessions, respectively. Intra-amygdala correlations were larger than correlations from the BNST to the amygdala. All partial correlations were distributed around zero, showing many connections with negative values of roughly equal strength.

3.6 | Robustness against hemispheric lateralization

As can be seen in Figure S4 (Supporting Information), the results of the DCMs that were estimated for each hemisphere separately were highly consistent with the DCM that did not differentiate between hemispheres. Thus, there seems to be no hemispheric lateralization in the EC between BNST and amygdala nuclei.

3.7 | Summary of results

Our results of the EC estimation between BNST and amygdala nuclei, using high-quality data from the HCP, revealed a fully interconnected system with asymmetric EC. That is, all amygdala nuclei were positively connected to each other but strongly inhibited the BNST, whereas the BNST showed positive EC to all amygdala nuclei. The

relative strength of the EC parameters between the nuclei was consistent over the two sessions, although the second session showed smaller EC values overall. The relative connectivity structure between amygdala nuclei and BNST was maintained when calculated for each hemisphere separately. We also found that males showed stronger EC from the LB to the BNST and the CM to the BNST, which was stable over the two sessions. In accordance with previous research, we found significant positive partial correlations between all nuclei. However, despite significance, the effect sizes were relatively small, with the BNST showing only minor correlations to amygdala nuclei. On the other hand, intra-amygdala correlations were larger. Our analysis of the impulse response of the system to an impulse into the LB, revealed partially antagonistic, out of phase dynamics between BNST and amygdala.

4 | DISCUSSION

Our analysis provides the first evidence for a fully interconnected and directed rsfMRI connectivity between amygdala nuclei and BNST. We thus add directivity to previous research that was solely based on the analysis of FC. Importantly, our analysis was based on a spectral DCM that takes the dynamic interactions between regions into account and provides an estimate of EC, that is, a more suitable measure of the true coupling between regions (Friston, 2011). In DCM for fMRI, the activity of a modeled region is an abstract representation of neuronal activity that corresponds to the amplitude of macroscopic variables summarizing the dynamics of large neuronal populations which generate a hemodynamic response (Friston et al., 2003). The ROI time series for the DCM are based on the principal component that explains the highest amount of variance, that is, the component which mostly dominates the internal dynamics of the blood oxygenation level dependent (BOLD) signal of all voxels within a given ROI. Thus, our data offer insight into the EC based on the population dynamics of thousands of neurons within a voxel generating the BOLD signal, which reflects local field potentials caused by excitatory/inhibitory postsynaptic potentials, dendritic afterhyperpolarizations, and membrane oscillations (Ekstrom, 2010; Logothetis, Pauls, Augath, Trinath, & Oeltermann, 2001). Our study, therefore, provides a macroscopic measure of connectivity and complements research that focussed on electrophysiological, pharmacogenetic, or optogenetic stimulation in rodents and primates uncovering the directed connectivity structure between the amygdala and the BNST on the cellular level.

Our finding of a fully interconnected system is in accordance with studies showing a close interaction between amygdala nuclei and BNST (e.g., Been & Petrulis, 2011; Dong et al., 2001; Duvarci & Pare, 2014; Gungor, Yamamoto, & Pare, 2015). However, a direct comparison between the results from microscopic research and our macroscopically orientated approach is difficult, and further research with detailed biophysically realistic models is required to establish a link between both approaches.

Our results show an asymmetric connectivity structure, such that the BNST is strongly negatively connected to all amygdala nuclei, but itself shows positive EC to these nuclei. This has not been uncovered in previous studies due to the use of symmetric measures of FC (Avery et al., 2014; Oler et al., 2012; Oler et al., 2017; Tillman et al., 2018; Torrisi et al., 2015). These studies revealed positively correlated BOLD signal fluctuations in the rsfMRI between amygdala nuclei and BNST, which we could reproduce as well (see Figure S1 and Tables S1 and S2, Supporting Information). However, although positive and significant, the BNST showed only minor partial correlations to the amygdala nuclei. For example, the partial correlation between the BNST and the CM was 0.007 in the first session and 0.01 in the second session. The correlations were mainly distributed around zero, with a high percentage of correlations also being negative (Figures S2 and S3, Supporting Information). Similarly, the intra-amygdala partial correlations were also distributed around zero, although slightly more shifted toward positive values. These results suggest a wide distribution of partial correlations with only small positive effect sizes. Since our sample size was comparatively larger than in previous studies and included 2,400 measurements for each session, the found partial correlations can be seen as more representative of the true effect sizes in the population (Button et al., 2013). Thus, this distribution of positive and negative correlations might reflect the more complicated underlying connectivity structure found with our EC analysis.

4.1 | Information processing in the BNST and amygdala is partially separated

Our DCM analysis further suggests that the amygdala forms a positively interconnected network that receives excitatory influence from the BNST, but itself inhibits it. Thus, while activity flow within the amygdala is highly correlated and informed by the BNST, activity flow in the BNST seems to be partially separated from the amygdala, since it will be inhibited when amygdala activity increases. On the one hand, this might point toward a crucial role of the amygdala in regulating BNST activity in the resting-state. Since the BNST has been found to be an important regulator of hypothalamic–pituitary–adrenal axis (HPA) activity (Choi et al., 2007), the strong negative EC might point toward a preponderance of neuronal connections that suppress BNST activity and thus the HPA axis. This suppression could serve the purpose of maintaining a relaxed, that is, anxiolytic state that is characterized by a relatively low level of arousal due to the absence of an overt task. On the other hand, these results point toward a partially antagonistic relationship between BNST and amygdala, that might be the result of segregated information processing in the resting-state. This segregated information processing could likely be mediated by integration into different cortical and subcortical networks. In addition, our simulation of the impulse response of the system confirms that the found EC generates partially antagonistic activity flow, and thus shows that there also exists a period where both BNST and amygdala are activated together. This overlap in their activity indicates that information processing is not entirely separated. Although further investigations with a larger number of brain regions are required to elucidate the specific EC-based network structure of BNST and amygdala, previous rsfMRI FC studies suggest different connectivity profiles for the BNST, the LB, CM, and SF. For example, the BNST has been found to be coupled to regions of the default mode network (Avery et al., 2014; Tillman et al., 2018; Torrisi et al., 2015), while the direct comparison between the BNST and the CM shows that the BNST is stronger connected to regions involved in the default mode network and the CM shows preferential coupling to

regions that coordinate responses to sensory stimuli (Gorka, Torrisi, Shackman, Grillon, & Ernst, 2018; Tillman et al., 2018).

Further evidence for segregated information processing of the BNST as compared to the amygdala comes from several other studies that investigated the BOLD activity during induced states of phasic and sustained fear in humans. Those studies found the BNST to be activated during sustained fear states caused by unpredictable threat conditions (Alvarez, Chen, Bodurka, Kaplan, & Grillon, 2011), in anticipation of threatening events (e.g., Klumpers, Kroes, Baas, & Fernández, 2017; Somerville, Whalen, & Kelley, 2010) or aversive stimuli (e.g., Brinkmann, Buff, Feldker, et al., 2017; Brinkmann, Buff, Neumeister, et al., 2017; Brinkmann et al., 2018; Grupe, Oathes, & Nitschke, 2013; Herrmann et al., 2016; Somerville et al., 2013; Straube, Mentzel, & Miltner, 2007). Thus, the initiation of a general, longer lasting state of apprehension before and after a challenge to homeostasis has occurred, rather than immediate reactions to specific threats, seems to be a key difference between the amygdala and the BNST (Davis et al., 2010). Specifically, Davis et al. (2010) proposed that a fear-eliciting stimulus rapidly activates the laterobasal amygdala and the medial part of the central amygdala and triggers a phasic fear response. This response is paralleled by activation of the lateral central amygdala that results in a release of corticotropin-releasing factor into the BNST to produce a more slowly acting sustained fear response. This phasic fear response is then turned off by inhibitory feedback from the BNST, and possibly the lateral central amygdala, to the medial central amygdala. Despite evidence from fMRI studies of a delayed and sustained BOLD activity of the BNST (Alvarez et al., 2011; Brinkmann, Buff, Feldker, et al., 2017; Brinkmann, Buff, Neumeister, et al., 2017; Herrmann et al., 2016; Straube et al., 2007), recent evidence also indicates a complex interaction between amygdala, such that both contribute to shaping phasic and sustained fear responses (for reviews, see Fox & Shackman, 2017; Gungor & Pare, 2016).

Although we are not able to provide a definite answer to the general discussion about the role of the BNST and the amygdala nuclei in phasic and sustained fear responses, the relative timings of these structures based on our simulation of the impulse response seems to support the observations of a delayed and longer lasting BNST activity. Specifically, as can be seen in Figure 4, the BNST is initially downregulated and increases its activity to a maximum 5.5 s after stimulus onset. Moreover, its activity amplitude is much higher relative to the amygdala nuclei and therefore takes longer to decay to zero.

The CM and SF, on the other hand, show a short initial peak after 0.8 s, followed by a strong downregulation of all nuclei with maximum amplitude after 3.7 s. Thus, while there is a short initial amygdala activation, the BNST shows a delayed upregulation starting 3.7 s after stimulus onset. As our data further indicate, the negative EC from the amygdala to the BNST is crucial for shaping this partially antagonistic (out of phase) and delayed upregulation of the BNST. The BNST shows an activity flow that is phase shifted around 90° to the activity flow of the amygdala nuclei. This relationship might, again, indicate separated information processing but also point toward a period of shared information processing. Importantly, this antagonistic relationship between BNST and amygdala does not seem to be the result of absent connections between them, since the results of the model comparison identified the fully connected model as the one that explains the data best. Rather, the interconnectivity between BNST and amygdala shapes this activity flow pattern in a dynamic manner. Our results, therefore, reveal a baseline connectivity structure that supports partially antagonistic information flow between BNST and amygdala nuclei.

However, it is likely that changes in the EC structure during certain tasks occur, which may alter the information flow between BNST and amygdala. Given the importance of resting-state connectivity in shaping task-evoked activity (Cole, Bassett, Power, Braver, & Petersen, 2014; Cole, Ito, Bassett, & Schultz, 2016), it would be interesting to investigate if the EC structure between BNST and amygdala during a task still generates antagonistic information flow or becomes more synchronized. Future research needs to investigate this question in more detail, for example, by using DCMs that allow for the estimation of modulatory changes in EC by task conditions.

4.2 | Influence of self-inhibition on activation decay

The estimated EC parameters also offer valuable insight into the strength of self-inhibition of the nuclei, which indicates the speed of signal decay in Hertz. Interestingly, our results show that the CM was most strongly self-inhibited in comparison to the other nuclei. Given the important role of this nucleus in mediating autonomic responses and arousal (Cardinal et al., 2002; Pessoa, 2011), this self-inhibition could be the result of the resting-state. That is, it might indicate a preponderance of inhibitory influence possibly mediated through the influence of the centrolateral nucleus onto the CM, that fosters a more relaxed anxiolytic state. It could also indicate that signals in the CM generally have a faster decay due to certain physiological properties of this nucleus. Here as well, it would be interesting to investigate further if the strength of self-inhibition is altered during certain tasks, for example, during threat confrontation or threat anticipation. On the other hand, the BNST showed a relatively small value of self-inhibition compared to the other nuclei. This indicates that a signal in the BNST is sustained for a longer time in the resting-state. It is noteworthy, however, that the speed of signal decay is heavily influenced by the other nuclei.

4.3 | Sex effects on EC parameters

We also investigated the relationship between EC parameters and age and sex. We did not find any effects of age on the EC parameters. However, there were effects of LB-BNST and CM-BNST EC in males whereas SF-BNST and SF-SF EC in females were not consistent over sessions. Thus, there was less inhibition of the LB-BNST and the CM-BNST EC in males, which may facilitate BNST activation by the LB and CM as well as other structures to which the BNST is connected. Although further research is required to untangle the influence of this differential connectivity structure on certain types of behavior (e.g., aggression, reproduction), our results add to previous research showing that the BNST exhibits volumetric, neurochemical and behavioral sexual dimorphism in animals and humans (Allen & Gorski, 1990; Hines et al., 1992).

4.4 | Implications for anxiety disorders

Given the known role of amygdala and BNST in mediating fear and anxiety responses (Avery, Clauss, & Blackford, 2016; Davis et al.,

2010), it is worth thinking about the possible implications of our results for anxiety disorders. As has been pointed out in this study, the BNST–amygdala circuit connectivity generates a time-dependent dynamics that shows a short initial (phasic) amygdala activation and a longer delayed (sustained) BNST activation in response to an impulse input into the LB. If this similarity is merely conicidental, needs to be further investigated, but such an interplay of phasic and sustained activation in amygdala and BNST has been observed in previous studies and seems highly relevant for fear and anxiety responses and indicative of a close interaction between these nuclei (Davis et al., 2010; Fox & Shackman, 2017).

As has been reported by several studies from our lab, exaggerated phasic amygdala and sustained BNST activity in reaction to aversive stimuli seems to be characteristic for anxiety disorders. For example, female patients with posttraumatic stress disorder as well as panic disorder patients and patients with generalized anxiety disorder showed increased initial phasic amygdala and increased sustained BNST fMRI BOLD responses during the anticipation of aversive versus neutral sounds as compared to controls (Brinkmann, Buff, Feldker, et al., 2017; Brinkmann, Buff, Neumeister, et al., 2017; Buff et al., 2017). Considering the vast amount of research investigating the neuroplasticity that goes along with fear/anxiety learning and expression (e.g., Cardinal et al., 2002; Davis et al., 2010; Duvarci & Pare, 2014), it is plausible that these exaggerated responses to aversive stimuli in patients are caused by specific alterations of the connectivity structure of processing regions, affecting, among others, the BNST–amygdala circuit. For example, increasing the EC strength between one or several amygdala nuclei (e.g., increasing the EC from CM to SF or LB to CM) in our DCM equations, results in a heightened initial amygdala amplitude as well as increased and longer lasting BNST amplitude in response to an impulse. In other words, elevated EC within the amygdala causes a stronger initial activation of LB, CM, and SF, which results in stronger deactivation of the BNST due to the inhibitory influence of the amygala nuclei. Subsequently, through the positive EC from BNST to amygdala, inhibition of the BNST leads to inhibition of the amygdala. This inhibition of the amygdala nuclei is then followed by a disinhibition of the BNST resulting in an increased activation amplitude and prolonged oscillatory activation decay.

Although a direct comparison between the results from fMRI BOLD activation studies and the impulse response of DCM equations is difficult; by altering the within amygdala EC in our model, it is possible to generate a pattern of increased neuronal activations in amygdala and BNST that shows similarities to what has been empirically observed in patients under conditions of threat anticipation. Therefore, despite the DCM being an abstract macroscopic representation of neuronal population dynamics, our found EC structure of the BNST–amygdala circuit seems to reflect some underlying dynamics between these nuclei.

This result becomes even more relevant since the resting-state connectivity structure has been found to be a baseline where only a small amount of connections are minimally altered during tasks (Cole et al., 2014). It is still an outstanding question, however, if patients show general EC alterations that are reflected in the resting-state connectivity pattern or if they only show extensive modulations of an otherwise normal (as compared to controls) connectivity within the BNST–amygdala circuit or both. Which connections are altered and/or modulated in clinical populations needs to be addressed in future studies investigating the task-modulated EC, ideally along with an estimation of the resting-state EC of the same subjects.

4.5 | No hemispheric lateralization in EC

Our results suggest no difference in the general EC pattern of amygdala and BNST between hemispheres (see Figure S4, Supporting Information). This absence of hemispheric differences in the resting-state EC is an interesting result, given that lateralization in the amygdala has been consistently reported, especially during emotion processing (Baas, Aleman, & Kahn, 2004; Sergerie, Chochol, & Armony, 2008). Therefore, one might suspect differences in connectivity between hemispheres as well. An explicit investigation of lateralization in EC between amygdala and BNST has not been done before, but a previous rsFC study by Gorka et al. (2018) tested for differences in FC of left/right BNST and CM and found significant effects in several cortical areas. However, in agreement with our results, they did not find any hemispheric differences in FC from BNST or CM to LB and SF. Therefore, in the resting-state, there seems to be no lateralization within our investigated circuitry. If this is also the case for task-modulated EC, especially during emotion processing, can not be answered yet and needs to be addressed in further studies. It is likely, however, that lateralization in amygdala activation during emotion processing is strongly dependent on the modulatory influence exerted by other cortical areas, which we did not include in our model.

5 | LIMITATIONS

Several limitations of this study have to be discussed. First, we did not explicitly model the EC between left and right hemispheric nuclei, that is, estimating a DCM with eight instead of four ROIs with separate time series for each hemisphere. There were two reasons for this: First, due to the small size of the structures, we wanted to maximize the signal-to-noise ratio and therefore chose to extract the principal component from as many voxels as possible, that is, the combined voxels of the regions of interest extracted from both hemispheres. Second, given the lack of previous research we did not have any specific hypotheses about the between hemispheric EC. However, in order to ensure that there is a similar EC pattern in each hemispheric, we calculated separate DCMs with the time series for each hemisphere, which produced comparable results (Figure S4, Supporting Information). Nonetheless, we do not know yet if the nuclei show different EC to the contralateral hemisphere, that is, if the left BNST differentially influences the left CM as compared to the right BNST. Further research is necessary to investigate this issue in more detail.

Also, we did only focus on calculating the EC between BNST and amygdala nuclei. Since the BNST and amygdala have afferents and efferents to a multitude of other brain regions, the EC reported does not take the influence of these other regions into account. Further studies need to include more regions to provide a more comprehensive assessment of the whole-brain EC structures of the BNST and amygdala. However, although recent developments have been proposed that

enable the calculation of DCMs (Frässle et al., 2017; Razi et al., 2017) with up to 66 regions, at the moment the computational burden of calculating large-scale DCMs is very high. Another limitation is the spatial resolution of the ROIs. The BNST is a heterogeneous structure consisting of several subnuclei that are involved in different functions (Gungor & Pare, 2016). For example, BNST subnuclei were found to be involved in opposing circuits that mediate anxiogenic and anxiolytic responses (Kim et al., 2013), fear learning (Haufler, Nagy, & Pare, 2013) or differentially regulate the HPA axis (Choi et al., 2007). Also, we did not distinguish between the centrolateral and centromedial amygdala, two subdivisions that also have been found to play essential differential roles in the mediation of fear and anxiety responses (Ciocchi et al., 2010; Davis et al., 2010; Duvarci & Pare, 2014). The same is true for a separation between the lateral, basal, and basomedial nuclei of the basolateral complex of the amygdala, which also have been shown to mediate different aspects of fear learning and fear expression (Duvarci & Pare, 2014). Our results are therefore limited since the signal components used in the DCM comprise a mixture of signals from several subnuclei. Further studies investigating the EC of these subnuclei, using high resolution 7 Tesla fMRI, might provide further insight into the different roles of these nuclei. However, at the moment, a distinction between BNST subnuclei as well as subnuclei of the central amygdala is not possible due to the limited spatial resolution of fMRI, although a recent work did differentiate subnuclei of the amygdala in greater detail than previously done (Tyszka & Pauli, 2016).

As a final note, our results only reflect the static estimated connectivity structure within the resting-state. However, the coupling between regions is most likely altered by external stimuli, and further research needs to investigate EC modulations by specific tasks. Moreover, future studies investigating the resting-state EC between healthy controls and patients, for example, with an anxiety disorder, might provide further insight into the alterations of EC due to certain disorders.

6 | CONCLUSION

Our study gives the first insight into the resting-state EC between BNST and amygdala nuclei and the relation of the EC with age and sex as well as the reproducibility over two sessions. We found that the BNST is positively connected to all amygdala nuclei while being strongly inhibited by all of them. Our results further suggest that this asymmetric EC generates a partially antagonistic (out of phase) dynamic interaction between these structures. We thus add directivity to previous research and provide a deeper insight into the coupling between BNST and amygdala nuclei that is model-based and does not rely on the estimation of connectivity based on statistical BOLD signal fluctuations.

ACKNOWLEDGMENTS

The authors are grateful to the support team of the Human Connectome Project. This work was supported by the German Research Foundation (DFG: SFB/TRR 58: C06, C07).

ORCID

David Hofmann https://orcid.org/0000-0003-3494-634X

REFERENCES

Ahrens, S., Wu, M., Furlan, A., Hwang, G.-R., Paik, R., Li, H., … Li, B. (2018). A central extended amygdala circuit that modulates anxiety. *The Journal of Neuroscience*, *38*, 0705–0718. http://www.ncbi.nlm.nih.gov/pubmed/29844022

Alarcón, G., Cservenka, A., Rudolph, M. D., Fair, D. A., & Nagel, B. J. (2015). Developmental sex differences in resting state functional connectivity of amygdala sub-regions. *Neuroimage*, *115*, 235–244. https://doi.org/10.1016/j.neuroimage.2015.04.013

Allen, L. S., & Gorski, R. A. (1990). Sex difference in the bed nucleus of the stria terminalis of the human brain. *The Journal of Comparative Neurology*, *302*, 697–706.

Alvarez, R. P., Chen, G., Bodurka, J., Kaplan, R., & Grillon, C. (2011). Phasic and sustained fear in humans elicits distinct patterns of brain activity. *NeuroImage*, *55*, 389–400. https://doi.org/10.1016/j.neuroimage.2010.11.057

Amunts, K., Kedo, O., Kindler, M., Pieperhoff, P., Mohlberg, H., Shah, N. J., … Zilles, K. (2005). Cytoarchitectonic mapping of the human amygdala, hippocampal region and entorhinal cortex: Intersubject variability and probability maps. *Anatomy and Embryology*, *210*, 343–352.

Avery, S. N., Clauss, J. A., & Blackford, J. U. (2016). The human BNST: Functional role in anxiety and addiction. *Neuropsychopharmacology*, *41*, 126–141. http://www.nature.com/doifinder/10.1038/npp.2015.185

Avery, S. N., Clauss, J. A., Winder, D. G., Woodward, N., Heckers, S., & Blackford, J. U. (2014). BNST neurocircuitry in humans. *NeuroImage*, *91*, 311–323. http://www.ncbi.nlm.nih.gov/pubmed/24444996

Baas, D., Aleman, A., & Kahn, R. S. (2004). Lateralization of amygdala activation: A systematic review of functional neuroimaging studies. *Brain Research Reviews*, *45*, 96–103.

Balleine, B. W., & Killcross, S. (2006). Parallel incentive processing: An integrated view of amygdala function. *Trends in Neurosciences*, *29*, 272–279.

Been, L. E., & Petrulis, A. (2011). Chemosensory and hormone information are relayed directly between the medial amygdala, posterior bed nucleus of the stria terminalis, and medial preoptic area in male Syrian hamsters. *Hormones and Behavior*, *59*, 536–548. https://doi.org/10.1016/j.yhbeh.2011.02.005

Bienkowski, M. S., & Rinaman, L. (2013). Common and distinct neural inputs to the medial central nucleus of the amygdala and anterior ventrolateral bed nucleus of stria terminalis in rats. *Brain Structure and Function*, *218*, 187–208.

Brinkmann, L., Buff, C., Feldker, K., Neumeister, P., Heitmann, C. Y., Hofmann, D., … Straube, T. (2018). Inter-individual differences in trait anxiety shape the functional connectivity between the bed nucleus of the stria terminalis and the amygdala during brief threat processing. *NeuroImage*, *166*, 110–116. https://doi.org/10.1016/j.neuroimage.2017.10.054

Brinkmann, L., Buff, C., Feldker, K., Tupak, S. V., Becker, M. P. I., Herrmann, M. J., & Straube, T. (2017). Distinct phasic and sustained brain responses and connectivity of amygdala and bed nucleus of the stria terminalis during threat anticipation in panic disorder. *Psychological Medicine*, *47*, 2675–2688.

Brinkmann, L., Buff, C., Neumeister, P., Tupak, S. V., Becker, M. P. I., Herrmann, M. J., & Straube, T. (2017). Dissociation between amygdala and bed nucleus of the stria terminalis during threat anticipation in female post-traumatic stress disorder patients. *Human Brain Mapping*, *38*, 2190–2205.

Buff, C., Brinkmann, L., Bruchmann, M., Becker, M. P. I., Tupak, S., Herrmann, M. J., & Straube, T. (2017). Activity alterations in the bed nucleus of the stria terminalis and amygdala during threat anticipation in generalized anxiety disorder. *Social Cognitive and Affective Neuroscience*, *12*, 1766–1774.

Bupesh, M., Abellán, A., & Medina, L. (2011). Genetic and experimental evidence supports the continuum of the central extended amygdala and a multiple embryonic origin of its principal neurons. *The Journal of Comparative Neurology*, *519*, 3507–3531.

Button, K. S., Ioannidis, J. P. A., Mokrysz, C., Nosek, B. A., Flint, J., Robinson, E. S. J., & Munafò, M. R. (2013). Power failure: Why small sample size undermines the reliability of neuroscience. *Nature Reviews. Neuroscience*, *14*, 365–376. http://www.ncbi.nlm.nih.gov/pubmed/23571845

Cardinal, R. N., Parkinson, J. A., Hall, J., & Everitt, B. J. (2002). Emotion and motivation: The role of the amygdala, ventral striatum, and prefrontal cortex. *Neuroscience and Biobehavioral Reviews*, *26*, 321–352.

Choi, D. C., Furay, A. R., Evanson, N. K., Ostrander, M. M., Ulrich-Lai, Y. M., & Herman, J. P. (2007). Bed nucleus of the stria terminalis subregions differentially regulate hypothalamic-pituitary-adrenal Axis activity: Implications for the integration of limbic inputs. *The Journal of Neuroscience*, *27*, 2025–2034. http://www.jneurosci.org/cgi/doi/10.1523/JNEUROSCI.4301-06.2007

Ciocchi, S., Herry, C., Grenier, F., Wolff, S. B. E., Letzkus, J. J., Vlachos, I., … Lüthi, A. (2010). Encoding of conditioned fear in central amygdala inhibitory circuits. *Nature*, *468*, 277–282.

Cole, M. W., Bassett, D. S., Power, J. D., Braver, T. S., & Petersen, S. E. (2014). Intrinsic and task-evoked network architectures of the human brain. *Neuron*, *83*, 238–251. https://doi.org/10.1016/j.neuron.2014.05.014

Cole, M. W., Ito, T., Bassett, D. S., & Schultz, D. H. (2016). Activity flow over resting-state networks shapes cognitive task activations. *bioRxiv*, *19*, 055194. http://biorxiv.org/lookup/doi/10.1101/055194

Cooke, B. M., & Simerly, R. B. (2005). Ontogeny of bidirectional connections between the medial nucleus of the amygdala and the principal bed nucleus of the stria terminalis in the rat. *The Journal of Comparative Neurology*, *489*, 42–58.

Davis, M., Walker, D. L., Miles, L., & Grillon, C. (2010). Phasic vs sustained fear in rats and humans: Role of the extended amygdala in fear vs anxiety. *Neuropsychopharmacology*, *35*, 105–135. http://www.nature.com/doifinder/10.1038/npp.2009.109

Dong, H. W., Petrovich, G. D., & Swanson, L. W. (2001). Topography of projections from amygdala to bed nuclei of the stria terminalis. *Brain Research Reviews*, *38*, 192–246.

Duvarci, S., & Pare, D. (2014). Amygdala microcircuits controlling learned fear. *Neuron*, *82*, 966–980. https://doi.org/10.1016/j.neuron.2014.04.042

Eickhoff, S. B., Stephan, K. E., Mohlberg, H., Grefkes, C., Fink, G. R., Amunts, K., & Zilles, K. (2005). A new SPM toolbox for combining probabilistic cytoarchitectonic maps and functional imaging data. *NeuroImage*, *25*, 1325–1335. http://www.ncbi.nlm.nih.gov/pubmed/15850749

Ekstrom, A. (2010). How and when the fMRI BOLD signal relates to underlying neural activity: The danger in dissociation. *Brain Research Reviews*, *62*, 233–244. https://doi.org/10.1016/j.brainresrev.2009.12.004

Engman, J., Linnman, C., Van Dijk, K. R. A., & Milad, M. R. (2016). Amygdala subnuclei resting-state functional connectivity sex and estrogen differences. *Psychoneuroendocrinology*, *63*, 34–42.

Fadok, J. P., Markovic, M., Tovote, P., & Lüthi, A. (2018). New perspectives on central amygdala function. *Current Opinion in Neurobiology*, *49*, 141–147.

Fox, A. S., Oler, J. A., Birn, R. M., Shackman, A. J., Alexander, A. L., & Kalin, N. H. (2018). Functional connectivity within the primate extended amygdala is heritable and associated with early-life anxious temperament. *The Journal of Neuroscience*, *38*, 0102–0118. http://www.jneurosci.org/lookup/doi/10.1523/JNEUROSCI.0102-18.2018

Fox, A. S., & Shackman, A. J. (2017). The central extended amygdala in fear and anxiety: Closing the gap between mechanistic and neuroimaging research. *Neuroscience Letters*, *693*, 58–67. https://doi.org/10.1016/j.neulet.2017.11.056

Frässle, S., Lomakina, E. I., Razi, A., Friston, K. J., Buhmann, J. M., & Stephan, K. E. (2017). Regression DCM for fMRI. *NeuroImage*, *155*, 406–421. https://doi.org/10.1016/j.neuroimage.2017.02.090

Friston, K. (2011). Functional and effective connectivity: a review. *Brain Connectivity*, *1*, 13–36. http://www.ncbi.nlm.nih.gov/pubmed/22432952

Friston, K. J., Harrison, L., & Penny, W. (2003). Dynamic causal modelling. *NeuroImage*, *19*, 1273–1302. http://linkinghub.elsevier.com/retrieve/pii/S1053811903002027

Friston, K. J., Kahan, J., Biswal, B., & Razi, A. (2014). A DCM for resting state fMRI. *Neuroimage*, *94*, 396–407. https://doi.org/10.1016/j.neuroimage.2013.12.009

Friston, K. J., Litvak, V., Oswal, A., Razi, A., Stephan, K. E., Van Wijk, B. C. M., … Zeidman, P. (2016). Bayesian model reduction and empirical Bayes for group (DCM) studies. *NeuroImage*, *128*, 413–431. https://doi.org/10.1016/j.neuroimage.2015.11.015

Gabard-Durnam, L. J., Flannery, J., Goff, B., Gee, D. G., Humphreys, K. L., Telzer, E., … Tottenham, N. (2014). The development of human amygdala functional connectivity at rest from 4 to 23years: A cross-sectional study. *NeuroImage*, *95*, 193–207. https://doi.org/10.1016/j.neuroimage.2014.03.038

Glasser, M. F., Smith, S. M., Marcus, D. S., Andersson, J. L. R., Auerbach, E. J., Behrens, T. E. J., … Van Essen, D. C. (2016). The Human Connectome Project's neuroimaging approach. *Nature Neuroscience*, *19*, 1175–1187.

Glasser, M. F., Sotiropoulos, S. N., Wilson, J. A., Coalson, T. S., Fischl, B., Andersson, J. L., … Jenkinson, M. (2013). The minimal preprocessing pipelines for the Human Connectome Project. *NeuroImage*, *80*, 105–124. http://www.ncbi.nlm.nih.gov/pubmed/23668970

Goossens, L., Kukolja, J., Onur, O. A., Fink, G. R., Maier, W., Griez, E., … Hurlemann, R. (2009). Selective processing of social stimuli in the superficial amygdala. *Human Brain Mapping*, *30*, 3332–3338.

Gorka, A. X., Torrisi, S., Shackman, A. J., Grillon, C., & Ernst, M. (2018). Intrinsic functional connectivity of the central nucleus of the amygdala and bed nucleus of the stria terminalis. *Neuroimage*, *168*, 392–402.

Griffanti, L., Salimi-Khorshidi, G., Beckmann, C. F., Auerbach, E. J., Douaud, G., Sexton, C. E., … Smith, S. M. (2014). ICA-based artefact removal and accelerated fMRI acquisition for improved resting state network imaging. *NeuroImage*, *95*, 232–247.

Grupe, D. W., Oathes, D. J., & Nitschke, J. B. (2013). Dissecting the anticipation of aversion reveals dissociable neural networks. *Cerebral Cortex*, *23*, 1874–1883. http://www.ncbi.nlm.nih.gov/pubmed/22763169

Gungor, N. Z., & Pare, D. (2016). Functional heterogeneity in the bed nucleus of the stria terminalis. *The Journal of Neuroscience*, *36*, 8038–8049. http://www.jneurosci.org/cgi/doi/10.1523/JNEUROSCI.0856-16.2016

Gungor, N. Z., Yamamoto, R., & Pare, D. (2015). Optogenetic study of the projections from the bed nucleus of the stria terminalis to the central amygdala. *Journal of Neurophysiology*, *114*, 2903–2911. http://jn.physiology.org/lookup/doi/10.1152/jn.00677.2015

Haufler, D., Nagy, F. Z., & Pare, D. (2013). Neuronal correlates of fear conditioning in the bed nucleus of the stria terminalis. *Learning & Memory*, *20*, 633–641. http://learnmem.cshlp.org/cgi/doi/10.1101/lm.031799.113

Herrmann, M. J., Boehme, S., Becker, M. P. I., Tupak, S. V., Guhn, A., Schmidt, B., … Straube, T. (2016). Phasic and sustained brain responses in the amygdala and the bed nucleus of the stria terminalis during threat anticipation. *Human Brain Mapping*, *37*, 1091–1102.

Hespanha, J. P. (2018). *Linear systems theory*. Princeton and Oxford: Princeton university press.

Hines, M., Allen, L. S., & Gorski, R. A. (1992). Sex differences in subregions of the medial nucleus of the amygdala and the bed nucleus of the stria terminalis of the rat. *Brain Research*, *579*, 321–326.

Kim, S.-Y., Adhikari, A., Lee, S. Y., Marshel, J. H., Kim, C. K., Mallory, C. S., … Deisseroth, K. (2013). Diverging neural pathways assemble a behavioural state from separable features in anxiety. *Nature*, *496*, 219–223. http://www.ncbi.nlm.nih.gov/pubmed/23515158

Klumpers, F., Kroes, M. C. W., Baas, J., & Fernández, G. (2017). How human amygdala and bed nucleus of the stria terminalis may drive distinct defensive responses. *The Journal of Neuroscience*, *37*, 3830–3816. http://www.jneurosci.org/lookup/doi/10.1523/JNEUROSCI.3830-16.2017

Koelsch, S., Skouras, S., Fritz, T., Herrera, P., Bonhage, C., Küssner, M. B., & Jacobs, A. M. (2013). The roles of superficial amygdala and auditory cortex in music-evoked fear and joy. *NeuroImage*, *81*, 49–60. https://doi.org/10.1016/j.neuroimage.2013.05.008

Krüger, O., Shiozawa, T., Kreifelts, B., Scheffler, K., & Ethofer, T. (2015). Three distinct fiber pathways of the bed nucleus of the stria terminalis to the amygdala and prefrontal cortex. *Cortex*, *66*, 60–68.

Lebow, M., & Chen, A. (2016). Overshadowed by the amygdala: The bed nucleus of the stria terminalis emerges as key to psychiatric disorders. *Molecular Psychiatry*, *21*, 450–463. http://www.nature.com/doifinder/10.1038/mp.2016.1

Logothetis, N. K., Pauls, J., Augath, M., Trinath, T., & Oeltermann, A. (2001). Neurophysiological investigation of the basis of the fMRI signal. *Nature*, *412*, 150–157. http://www.ncbi.nlm.nih.gov/pubmed/11449264

Maras, P. M., & Petrulis, A. (2008). The posteromedial cortical amygdala regulates copulatory behavior, but not sexual odor preference, in the male Syrian hamster (*Mesocricetus auratus*). *Neuroscience*, *156*, 425–435.

Nagy, F. Z., & Paré, D. (2008). Timing of impulses from the central amygdala and bed nucleus of the stria terminalis to the brain stem. *Journal of Neurophysiology*, *100*, 3429–3436.

Namburi, P., Beyeler, A., Yorozu, S., Calhoon, G. G., Halbert, S. A., Wichmann, R., … Tye, K. M. (2015). A circuit mechanism for

differentiating positive and negative associations. *Nature*, *520*, 675–678. http://www.nature.com/doifinder/10.1038/nature14366

Oler, J. A., Birn, R. M., Patriat, R., Fox, A. S., Shelton, S. E., Burghy, C. A., … Kalin, N. H. (2012). Evidence for coordinated functional activity within the extended amygdala of non-human and human primates. *Brain NeuroImage*, *61*, 1059–1066. https://doi.org/10.1016/j.neuroimage.2012.03.045

Oler, J. A., Tromp, D. P. M., Fox, A. S., Kovner, R., Davidson, R. J., Alexander, A. L., … Fudge, J. L. (2017). Connectivity between the central nucleus of the amygdala and the bed nucleus of the stria terminalis in the non-human primate: Neuronal tract tracing and developmental neuroimaging studies. *Brain Structure and Function*, *222*, 21–39.

Pessoa, L. (2011). Reprint of: Emotion and cognition and the amygdala: From " what is it?" to " what's to be done?". *Neuropsychologia*, *49*, 681–694.

Razi, A., Kahan, J., Rees, G., & Friston, K. J. (2014). Construct validation of a DCM for resting state fMRI. *NeuroImage*, *106*, 1–14. http://linkinghub.elsevier.com/retrieve/pii/S1053811914009446

Razi, A., Seghier, M. L., Zhou, Y., McColgan, P., Zeidman, P., Park, H.-J., … Friston, K. J. (2017). Large-scale DCMs for resting-state fMRI. *Network Neuroscience*, *1*, 222–241.

Root, C. M., Denny, C. A., Hen, R., & Axel, R. (2014). The participation of cortical amygdala in innate, odour-driven behaviour. *Nature*, *515*, 269–273.

Sah, P., Faber, E. L. S., Lopez De Armentia, M., & Power, J. (2003). The amygdaloid complex: Anatomy and physiology. *Physiological Reviews*, *83*, 803–834.

Salimi-Khorshidi, G., Douaud, G., Beckmann, C. F., Glasser, M. F., Griffanti, L., & Smith, S. M. (2014). Automatic denoising of functional MRI data: Combining independent component analysis and hierarchical fusion of classifiers. *NeuroImage*, *90*, 449–468. https://doi.org/10.1016/j.neuroimage.2013.11.046

Sergerie, K., Chochol, C., & Armony, J. L. (2008). The role of the amygdala in emotional processing: A quantitative meta-analysis of functional neuroimaging studies. *Neuroscience & Biobehavioral Reviews*, *32*(4), 811–830.

Skouras, S., Gray, M., Critchley, H., & Koelsch, S. (2014). Superficial amygdala and hippocampal activity during affective music listening observed at 3 T but not 1.5 T fMRI. *NeuroImage*, *101*, 364–369. https://doi.org/10.1016/j.neuroimage.2014.07.007

Smith, S. M., Beckmann, C. F., Andersson, J., Auerbach, E. J., Bijsterbosch, J., Douaud, G., … Glasser, M. F. (2013). Resting-state fMRI in the Human Connectome Project. *NeuroImage*, *80*, 144–168.

Somerville, L. H., Wagner, D. D., Wig, G. S., Moran, J. M., Whalen, P. J., & Kelley, W. M. (2013). Interactions between transient and sustained neural signals support the generation and regulation of anxious emotion. *Cerebral Cortex*, *23*, 49–60.

Somerville, L. H., Whalen, P. J., & Kelley, W. M. (2010). Human bed nucleus of the stria terminalis indexes hypervigilant threat monitoring. *Biological Psychiatry*, *68*, 416–424.

Straube, T., Mentzel, H.-J., & Miltner, W. H. R. (2007). Waiting for spiders: Brain activation during anticipatory anxiety in spider phobics. *NeuroImage*, *37*, 1427–1436. http://www.ncbi.nlm.nih.gov/pubmed/17681799

Sun, N., Roberts, L., & Cassell, M. D. (1991). Rat central amygdaloid nucleus projections to the bed nucleus of the stria terminalis. *Brain Research Bulletin*, *27*, 651–662.

Tillman, R. M., Stockbridge, M. D., Nacewicz, B. M., Torrisi, S., Fox, A. S., Smith, J. F., & Shackman, A. J. (2018). Intrinsic functional connectivity of the central extended amygdala. *Human Brain Mapping*, *39*, 1291–1312. https://doi.org/10.1002/hbm.23917

Torrisi, S., Gorka, A. X., Gonzalez-Castillo, J., O'Connell, K., Balderston, N., Grillon, C., & Ernst, M. (2018). Extended amygdala connectivity changes during sustained shock anticipation. *Translational psychiatry*, *8*(1), 33.

Torrisi, S., O'Connell, K., Davis, A., Reynolds, R., Balderston, N., Fudge, J. L., … Ernst, M. (2015). Resting state connectivity of the bed nucleus of the stria terminalis at ultra-high field. *Human Brain Mapping*, *36*, 4076–4088.

Tye, K. M., Prakash, R., Kim, S. Y., Fenno, L. E., Grosenick, L., Zarabi, H., … Deisseroth, K. (2011). Amygdala circuitry mediating reversible and bidirectional control of anxiety. *Nature*, *471*, 358–362. https://doi.org/10.1038/nature09820

Tyszka, J. M., & Pauli, W. M. (2016). In vivo delineation of subdivisions of the human amygdaloid complex in a high-resolution group template. *Human Brain Mapping*, *37*, 3979–3998.

Van Essen, D. C., Smith, S. M., Barch, D. M., Behrens, T. E. J., Yacoub, E., & Ugurbil, K. (2013). The WU-Minn Human Connectome Project: An overview. *NeuroImage*, *80*, 62–79. http://www.ncbi.nlm.nih.gov/pubmed/23684880

Waraczynski, M. (2016). Toward a systems-oriented approach to the role of the extended amygdala in adaptive responding. *Neuroscience and Biobehavioral Reviews*, *68*, 177–194. https://doi.org/10.1016/j.neubiorev.2016.05.015

Weller, K. L., & Smith, D. A. (1982). Afferent connections to the bed nucleus of the stria terminalis. *Brain Research*, *232*, 255–270.

Yu, K., Ahrens, S., Zhang, X., Schiff, H., Ramakrishnan, C., Fenno, L., … He, M. (2017). The central amygdala controls learning in the lateral amygdala. *Nature neuroscience*, *20*(12), 1680–1685.

SUPPORTING INFORMATION

Additional supporting information may be found online in the Supporting Information section at the end of this article.

How to cite this article: Hofmann D, Straube T. Resting-state fMRI effective connectivity between the bed nucleus of the stria terminalis and amygdala nuclei. *Hum Brain Mapp*. 2019; 40:2723–2735. https://doi.org/10.1002/hbm.24555